SIAM J. SCI. COMPUT.
Vol. 25, No. 5, pp. 1534–1556

DIRECT EVALUATION OF HYPERSINGULAR GALERKIN SURFACE INTEGRALS*

L. J. GRAY†, J. M. GLAESER‡, AND T. KAPLAN†

Abstract. A *direct* algorithm for evaluating hypersingular integrals arising in a three-dimensional Galerkin boundary integral analysis is presented. The singular integrals are defined as limits to the boundary, and by integrating two of the four dimensions analytically, the coincident integral is shown to be divergent. However, the divergent terms can be explicitly calculated and shown to cancel with corresponding singularities in the adjacent edge integrals. A single analytic integration is employed for the edge and vertex singular integrals. This is sufficient to display the divergent term in the edge-adjacent integral and to show that the vertex integral is finite. By explicitly identifying the divergent quantities, we can compute the hypersingular integral without recourse to Stokes's theorem or the Hadamard finite part. The algorithms are developed in the context of a linear element approximation for the Laplace equation but are expected to be generally applicable. As an example, the algorithms are applied to solve a thermal problem in an exponentially graded material.

Key words. boundary integral method, hypersingular integrals, Galerkin approximation, Laplace equation

AMS subject classifications. 65R20, 45E99

DOI. 10.1137/S1064827502405999

1. Introduction.

The Galerkin approximation of boundary integral equations, well studied theoretically [57], has become increasing popular in computational work. In particular, the symmetric-Galerkin approximation (a few basic references are [27, 30, 39, 41, 58, 59]; the review [6] has more complete citations) has two key advantages. First, as the name implies, the resulting coefficient matrix is symmetric, which is physically appealing [40] and allows for symmetric coupling with finite elements [29]. Second, with the Galerkin approach, integrals involving two derivatives of the Green's function, termed *hypersingular*, can be evaluated using standard continuous C^0 elements. This is in contrast to collocation, where existence of the hypersingular integral requires either C^1 elements or a discontinuous nonconforming interpolation; see [10, 15, 24, 32, 46, 47] for a more complete discussion of this issue. A recent survey of singular integration methods for both Galerkin and collocation can be found in [60].

The ability to work effectively with hypersingular equations is of importance beyond symmetric-Galerkin. These equations are essential for viable treatment of crack problems [5, 7, 58] and the postprocessing evaluation of surface stress [20].

*Received by the editors April 18, 2002; accepted for publication (in revised form) July 18, 2003; published electronically March 3, 2004. This work was supported in part by the Applied Mathematical Sciences Research Program of the Office of Mathematical, Information, and Computational Sciences, U.S. Department of Energy, under contract DE-AC05-00OR22725 with UT-Battelle, LLC. Additional support from the Office of Science's Scientific Discovery through Advanced Computing Program (SCIDAC) and the Office of Advanced Scientific Computing Research is gratefully acknowledged. The submitted manuscript was authored by a contractor of the U.S. Government under contract DE-AC05-00OR22725. The U.S. Government retains a nonexclusive, royalty-free license to publish or reproduce the published form of this contribution, or allow others to do so, for U.S. Government purposes.

http://www.siam.org/journals/sisc/25-5/40599.html

†Computer Science and Mathematics Division, Oak Ridge National Laboratory, Oak Ridge, TN 37831-6367 (ljg@ornl.gov, tsk@ornl.gov).

‡Lockheed Martin Naval Electronic & Surveillance Systems, Moorestown, NJ 08057 (julia.glaeser@lmco.com). This author was supported by the DOE Higher Education Research Experience Program at Oak Ridge National Laboratory.

They have proved useful for error estimation methods [51] and other areas as well. It is therefore important to have effective techniques for evaluating Galerkin integrals of hypersingular kernels.

Singular integrals are present because the Green's function $G(P, Q)$ and its derivatives diverge as $Q \to P$. In a Galerkin approximation, the integration of these functions is carried out with respect to both Q and P, and in terms of the numerical implementation, this means that integrations are required for every pair of elements $\{E_P, E_Q\}$. An integral is therefore singular if the elements are *coincident* ($E_P = E_Q$) or are *adjacent*, sharing either an edge or a vertex.

In two dimensions, the treatment of hypersingular integrals is reasonably straightforward, and several successful methods are available [8, 13, 31, 56]. A "direct" approach presented in [16] demonstrated that the coincident and adjacent singular integrals are not separately finite and that, as expected, the divergences cancel when the integrals are added. It is, moreover, a relatively simple matter to explicitly identify and remove the singularities, clearly essential for a numerical implementation. In the adjacent singular integration, the divergent terms occur only at a single point (the point common to the two elements), and as a consequence, they appear after a single, comparatively simple, analytic integration is carried out.

The situation in three dimensions is naturally much more complicated, as singularities now appear all along the edge shared by two elements. The predominant technique for handling the hypersingular integral has been to reformulate it using Stokes's theorem [11, 12, 37]. (Stokes's theorem is also the basis for a modified boundary element procedure called the boundary contour method [38, 49, 50].) In this approach the divergences disappear through the exact cancellation of contour integrals having opposite orientations. However, one must be able to perform the integration by parts. For the traditional Green's functions in computational mechanics, executing the Stokes transformation will not be a problem. For nonstandard applications, e.g., functionally graded materials [3, 19, 43, 44], it is likely to be possible, but also quite complicated. Thus, the development of a non-Stokes "direct" algorithm is of interest.

There are two additional important reasons for pursuing a direct evaluation procedure. First, due to simpler remeshing, the boundary integral method can be a highly effective technique for a wide range of moving boundary problems [23, 25, 42, 53]. However, computing the velocity of the surface usually requires complete knowledge of the function derivatives (e.g., gradient of potential, stress tensor) on the surface, and the boundary integral expressions for these quantities involve hypersingular kernels. As discussed elsewhere [22], direct limit evaluation leads to an accurate and highly efficient algorithm for computing these derivatives.

Second, even though the algorithms will be presented in the simplest context, the Laplace Green's function and a linear element approximation, the direct method appears to be completely general. This is supported by recent work applying these methods to the more complicated Green's functions for anisotropic elasticity [17] and graded materials [61]; the solution of a thermal problem in a graded material will be discussed below. Moreover, as demonstrated in [16] for two dimensions, the treatment of a higher order interpolation can be based upon the linear element procedures. The details of the analysis for a curved element in three dimensions are somewhat different and will be presented separately.

It will be demonstrated herein that the three-dimensional coincident and adjacent edge hypersingular integrals are separately divergent. To our knowledge, this has

not been previously established, though this must have been at least part of the motivation for the Stokes procedure. A direct evaluation must explicitly confront these divergences: it goes without saying that an algorithm must evaluate *finite* integrals; i.e., the divergent terms are, as in the Stokes procedure, removed exactly. Recently, two different direct evaluation approaches have been suggested, though a common theme is to exploit analytic integration. In [1, 9, 54, 55] exact integration is employed together with the Hadamard finite part definition [26] to assign finite values to the nonexistent integrals. The finite part definition of hypersingular integrals has a long history in boundary integral analysis [33, 34, 45]. In an alternate direct procedure presented in [18], the divergent coincident and adjacent edge integrals are first forced to be finite by moving the source point P off the boundary a distance ϵ [14, 21]. After (partial) analytic integration, the divergent terms of the form $\log(\epsilon)$ explicitly appear and can be seen to cancel when all integrals are added. Taking the limit $\epsilon \to 0$ back to the boundary then results in finite expressions and obviates the need for the Hadamard finite part.

In addition to the fundamental difference in the definition of the integrals, finite part versus limit, the strategies for analytic integration also differ significantly. With the finite part method, the inner integral is treated exactly, and the outer integration handled numerically. In [18] and herein, the analytic integration is always with respect to *the distance from the singularity*, accomplished by means of appropriate polar coordinate transformations. As a consequence, both the inner and outer integrals are handled partially analytically and partially numerically.

The limit analysis in [18] was tremendously simplified in that the (linear) elements were chosen to be identical to the parameter space; the purpose therein was solely to demonstrate that the divergent terms could be seen explicitly. Thus, while serving as a simple instructive exercise, [18] is far short of a complete and general algorithm. Nevertheless, a perusal of this previous paper would likely be a good preparation for going through the details herein.

Finally note that while the focus in this paper is on the hypersingular kernel, the techniques presented can also be applied to the less singular integrals involving the Green's function and its first derivative. The integrals of these functions are finite, no divergent terms arising in the boundary limit, and thus other approaches could be employed. However, the techniques described herein apply and are effective for these integrals as well. In the test calculations presented below, this approach will be adopted.

A synopsis of the paper is as follows. A brief review of background material on the Galerkin approximation of the hypersingular (Laplace) equation is provided in the next section. The subsequent three sections analyze the coincident, adjacent edge, and adjacent vertex integrals. The two basic techniques employed are, first, defining the integrals as boundary limits and, second, constructing appropriate polar coordinate transformations in the parameter spaces that are centered at the singularity. Specifically, the source point P is moved off the boundary a distance ϵ, and the limit $\epsilon \to 0$ is considered after analytic integration of the radial polar coordinate. For the coincident and adjacent edge cases, the integrations produce $\log(\epsilon)$ divergent terms, and the proof that these quantities mutually cancel is provided in section 6. The proof is simply brute force, evaluating the integrals that multiply the $\log(\epsilon)$ terms. The correctness of these algorithms is confirmed by results from three test calculations presented in section 7, one of which involves the Green's function for an exponentially graded material. The hypersingular kernel in this case is considerably more complicated than its counterpart for the Laplace equation.

2. Hypersingular equation. The purpose of this section is to define the quantity of interest, the Galerkin hypersingular integral for the Laplace equation, and to set the notation used throughout. A good reference for this material is the recent book by Bonnet [4].

The hypersingular boundary integral equation for the Laplace equation $\nabla^2\phi = 0$ is an expression for the surface flux $\partial\phi/\partial\mathbf{n} = \nabla\phi\bullet\mathbf{n}$, usually written in the form

$$\frac{\partial\phi}{\partial\mathbf{N}}(P) + \int_\Sigma \phi(Q)\frac{\partial^2 G}{\partial\mathbf{N}\partial\mathbf{n}}(P,Q)\,\mathrm{d}Q - \int_\Sigma \frac{\partial G}{\partial\mathbf{N}}(P,Q)\frac{\partial\phi}{\partial\mathbf{n}}(Q)\,\mathrm{d}Q = 0\ . \tag{1}$$

Here $\mathbf{n} = \mathbf{n}(Q)$, $\mathbf{N} = \mathbf{N}(P)$ denote the *outward* unit normal on the boundary surface Σ, and P and Q points on Σ. The fundamental solution $G(P,Q)$ is usually taken as the point source potential

$$G(P,Q) = \frac{1}{4\pi r}\ , \tag{2}$$

where $R = Q - P$ and $r = \|R\|$ is the distance between P and Q. The kernel functions in (1) are given by

$$\begin{aligned}\frac{\partial G}{\partial\mathbf{N}}(P,Q) &= \frac{1}{4\pi}\frac{\mathbf{N}\bullet R}{r^3}\ ,\\ \frac{\partial^2 G}{\partial\mathbf{N}\partial\mathbf{n}}(P,Q) &= \frac{1}{4\pi}\left(\frac{\mathbf{n}\bullet\mathbf{N}}{r^3} - 3\frac{(\mathbf{n}\bullet R)(\mathbf{N}\bullet R)}{r^5}\right)\ ,\end{aligned} \tag{3}$$

the second function being termed *hypersingular*. In potential theory, the integral of the first derivative is called a double layer potential; there doesn't appear to be a corresponding nomenclature for the hypersingular kernel. It is important to note that (1) is formally obtained by differentiating the standard boundary integral equation for surface potential,

$$\phi(P) + \int_\Sigma \left[\phi(Q)\frac{\partial G}{\partial\mathbf{n}}(P,Q) - G(P,Q)\frac{\partial\phi}{\partial\mathbf{n}}(Q)\right]\,\mathrm{d}Q = 0\ , \tag{4}$$

and then interchanging the derivative with the integral. As discussed in [14, 21], this interchange is in fact illegal, due to the singularity in the integrand. One way to legally reorder and therefore to legitimize (1) is to first write the surface potential equation with P off the boundary. As the kernel function is now well-behaved, the differentiation can be moved under the integral sign; the limit as P returns to the boundary can then be considered. This limit process will be employed below.

A side benefit of the direct limit procedure is that if the limit is taken with the source point P approaching the boundary from *outside* the domain, then the "free term" $\partial\phi(P)/\partial\mathbf{N}$ from (1) is not present (and thus normalization of the Green's function becomes unimportant). Assuming this exterior limit, (1) takes the form

$$\mathcal{F}(P) \equiv \int_\Sigma \phi(Q)\frac{\partial^2 G}{\partial\mathbf{N}\partial\mathbf{n}}(P,Q)\,\mathrm{d}Q - \int_\Sigma \frac{\partial G}{\partial\mathbf{N}}(P,Q)\frac{\partial\phi}{\partial\mathbf{n}}(Q)\,\mathrm{d}Q = 0\ , \tag{5}$$

with the free term automatically incorporated in the limit evaluation of the second integral in this equation. A separate computation of this term is therefore avoided. Note that the hypersingular integral is continuous as P crosses the boundary and is therefore the same whether an interior or exterior limit is used.

Following standard practice, we approximate the boundary potential and flux in terms of values at element nodes Q_j and shape functions $\psi_j(Q)$, i.e.,

$$\phi(Q) = \sum_j \phi(Q_j)\psi_j(Q),$$
$$\frac{\partial\phi}{\partial\mathbf{n}}(Q) = \sum_j \frac{\partial\phi}{\partial\mathbf{n}}(Q_j)\psi_j(Q)\ . \tag{6}$$

In a Galerkin approximation, these shape functions are employed to define weighting functions to enforce the integral equations. Specifically (5) becomes

$$\int_\Sigma \hat{\psi}_k(P)\mathcal{F}(P)\,\mathrm{d}P = 0, \tag{7}$$

where the weight function $\hat{\psi}_k(P)$ consists of all shape functions $\psi_l(P)$ that are nonzero at a particular node P_k. The weight function $\hat{\psi}_k(P)$ therefore has limited support, being nonzero only on the elements containing P_k.

For a particular element E_P for the outer P integration, singular integrals (i.e., when $Q = P$) occur if the Q-element either is coincident with E_P or shares a common edge or vertex with E_P. The evaluation of these integrals is discussed in detail herein. Unlike the coincident and edge-adjacent, the vertex-adjacent hypersingular integral will turn out to have a finite limit. Nevertheless, it can be effectively evaluated using the same techniques as used for the edge-adjacent case.

A linear element calculation will be analyzed in detail, as this forms the basis for handling higher order interpolations. An equilateral triangle parameter space $\{\eta, \xi\}$, where $-1 \le \eta \le 1$, $0 \le \xi \le \sqrt{3}(1-|\eta|)$, will be employed to construct approximations to the boundary and the boundary functions. This somewhat nonstandard choice of parameter space is convenient for executing the coincident integration, as will be explained in the next section. The three linear shape functions are

$$\psi_1(\eta,\xi) = \frac{\sqrt{3}(1-\eta)-\xi}{2\sqrt{3}},$$
$$\psi_2(\eta,\xi) = \frac{\sqrt{3}(1+\eta)-\xi}{2\sqrt{3}}, \tag{8}$$
$$\psi_3(\eta,\xi) = \frac{\xi}{\sqrt{3}}\ .$$

For an element defined by nodal points $\{Q_j = (x_j, y_j, z_j)\}$, the mapping from parameter space to the approximate boundary surface is

$$\Sigma(\eta,\xi) = \sum_{j=1}^{3}(x_j, y_j, z_j)\psi_j(\eta,\xi)\ , \tag{9}$$

and the corresponding surface potential is

$$\phi(\eta,\xi) = \sum_{j=1}^{3}\phi(Q_j)\psi_j(\eta,\xi)\ . \tag{10}$$

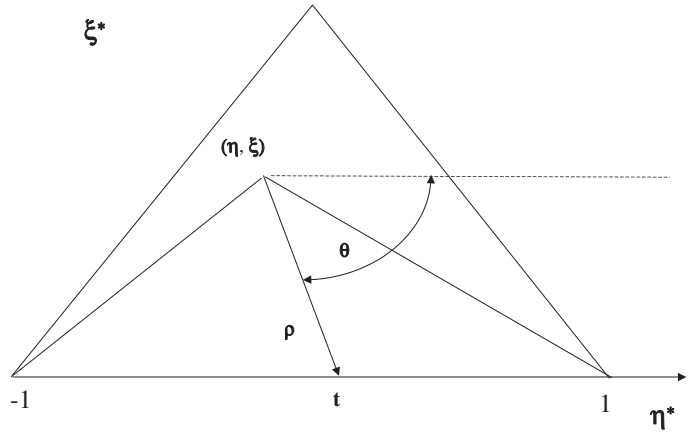

FIG. 1. *First polar coordinate transformation, $\{\eta^*, \xi^*\} \to \{\rho, \theta\}$, for the coincident integration. The variable t eventually replaces θ.*

3. Coincident integration. In the following we consider only the integration of the hypersingular kernel in (3). The integration of G or its first derivative can be handled in exactly the same manner, with the added simplification that no divergent terms appear in the $\epsilon \to 0$ limit.

For $E_P = E_Q = E$, the coincident integral to be evaluated is

$$\int_E \psi_k(P) \int_E \phi(Q) \frac{\partial^2 G}{\partial \mathbf{N} \partial \mathbf{n}}(P,Q)\, \mathrm{d}Q\, \mathrm{d}P = \sum_{j=1}^{3} \phi(Q_j) \int_E \psi_k(P) \int_E \psi_j(Q) \frac{\partial^2 G}{\partial \mathbf{N} \partial \mathbf{n}}(P,Q)\, \mathrm{d}Q\, dP\ , \tag{11}$$

where E is defined by nodes P_k, $1 \le k \le 3$. Transferring the integral to parameter space requires including the (constant) Jacobian J_P $(= J_Q)$, conveniently incorporated into the hypersingular kernel,

$$J_P^2 \frac{\partial^2 G}{\partial \mathbf{N} \partial \mathbf{n}}(P,Q) = \frac{1}{4\pi} \left(\frac{J_P^2}{r^3} - 3 \frac{(J_P N \bullet R)^2}{r^5} \right)\ . \tag{12}$$

The parametric variables for the outer P integration will be denoted by (η, ξ), and that for Q by (η^*, ξ^*). For the inner Q integration, the first step is to define a polar coordinate system centered at $P = (\eta, \xi)$,

$$\eta^* - \eta = \rho \cos(\theta), \tag{13}$$

$$\xi^* - \xi = \rho \sin(\theta), \tag{14}$$

as illustrated in Figure 1. Polar coordinate transformations, centered at the singularity, are particularly effective, as the Jacobian of the transformation $\rho\, d\rho$ reduces the order of the singularity. This will be exploited in all integrations.

As the expression for the upper limit of ρ, $\rho_L(\theta)$, is different as θ traverses each edge, the (ρ, θ) integration must be split into three subtriangles. In the following, we carry out the calculation for the lower subtriangle associated with the edge $\xi^* = 0$.

Although the remaining two cases could be handled in exactly the same manner, this would require repeating the analysis below for these two subtriangles. An alternate route, which has the benefit of simplifying the implementation, is to exploit the symmetry of the equilateral parameter space: the remaining subtriangles are handled by rotating the element and employing the formulas for the lower subtriangle. Compared to computing the integrals over all three subtriangles at the same time, this does create some small additional computational overhead. However, compared to the $\mathcal{O}(M^2)$ work required for the nonsingular integrals (M the number of elements), the coincident integrals are not a major contributor to the total computational cost. Thus, this is not a serious expense.

For this lower subtriangle, the integration limits are $0 \le \rho \le \rho_L$ and $\Theta_1 \le \theta \le \Theta_2$, where

$$\begin{aligned} \rho_L &= -\frac{\xi}{\sin(\theta)}, \\ \Theta_1 &= -\frac{\pi}{2} - \tan^{-1}\left(\frac{1+\eta}{\xi}\right), \\ \Theta_2 &= -\frac{\pi}{2} + \tan^{-1}\left(\frac{1-\eta}{\xi}\right). \end{aligned} \tag{15}$$

The distance $r = \|Q - P\|$, with P replaced by $P + \epsilon\mathbf{N}$ for the exterior boundary limit, takes the simple form

$$r^2(\rho,\theta) = \epsilon^2 + a^2(\theta)\rho^2 \ , \tag{16}$$

where

$$a^2 = a_{cc}\cos(\theta)^2 + a_{cs}\cos(\theta)\sin(\theta) + a_{ss}\sin(\theta)^2 \tag{17}$$

and the three coefficients $a_{\alpha\beta}$, α, $\beta = c, s$ depend solely on the coordinates of the element nodes (a^2 is in fact a positive quantity). With (13), the shape function $\psi_j(Q)$ becomes a linear function of ρ,

$$\psi_j(\rho,\theta) = c_{j,0}(\eta,\xi) + c_{j,1}(\eta,\xi,\theta)\rho \tag{18}$$

($c_{j,0}(\eta,\xi) = \psi_j(P)$). (To simplify the expressions that follow, the arguments will be dropped and the coefficients denoted simply as a, $c_{j,0}$, and $c_{j,1}$.) Thus, employing the boundary limit procedure and expressing the kernel function in polar coordinates, the hypersingular integral in (11) becomes

$$\begin{aligned} &\frac{J_P^2}{4\pi}\sum_{m=0}^{1}\int_{-1}^{1}\mathrm{d}\eta\int_{0}^{\sqrt{3}(1-|\eta|)}\psi_k(\eta,\xi)\,\mathrm{d}\xi\int_{\Theta_1}^{\Theta_2}c_{j,m}\,\mathrm{d}\theta \\ &\qquad\times\int_0^{\rho_L}\rho^{m+1}\left(\frac{1}{(a^2\rho^2+\epsilon^2)^{3/2}} - 3\frac{\epsilon^2}{(a^2\rho^2+\epsilon^2)^{5/2}}\right)\mathrm{d}\rho \ . \end{aligned} \tag{19}$$

The ρ integral is easily evaluated analytically. For $m = 0$ this results in

$$F_0 = -\frac{\rho_L^2}{(\,\epsilon^2 + a^2\,\rho_L^2\,)^{3/2}} \ , \tag{20}$$

while for $m = 1$

$$F_1 = -\frac{1}{a^3}\left[\log(\,\epsilon\,) - \log\left(a\rho_L + \sqrt{\epsilon^2 + a^2\rho_L^2}\right) + \frac{2a^3\rho_L^3 + \epsilon^2 a\rho_L}{(\epsilon^2 + a^2\rho_L^2)^{3/2}}\right] \ . \tag{21}$$

The $\log(\,\epsilon\,)$ term that appears in F_1 is *not* the divergent term that is being sought;

it can be seen to vanish in the subsequent θ integration. Note that this term is independent of ρ_L, and thus the complete integration over $0 \le \theta \le 2\pi$ can be considered. As the coefficient $c_{j,1}(\eta,\xi,\theta)$ is linear in $\cos(\theta)$ and $\sin(\theta)$, it satisfies $c_{j,1}(\eta,\xi,\pi+\theta) = -c_{j,1}(\eta,\xi,\theta)$. In addition, from (17), $a(\pi+\theta) = a(\theta)$, and thus

$$-\log(\epsilon)\int_0^{2\pi} \frac{c_{j,1}(\eta,\xi,\theta)}{a^3}\,\mathrm{d}\theta = 0\ . \tag{22}$$

Removing this $\log(\,\epsilon\,)$ term and then safely setting $\epsilon = 0$ in (21), the appropriate formula for $m = 1$ is

$$F_1 = -\frac{2 - \log(\,2a\rho_L\,)}{a^3} \tag{23}$$

(and in fact the $2/a^3$ term could be dropped, as the same argument shows that it too will integrate to zero).

This first analytic integration is not sufficient to display the divergent term. Note that for $\xi \approx 0$ in the subsequent integration, $\rho_L \approx 0$, and thus the singularities in F_0 and F_1 at $\rho_L = 0$ are of interest. The weak (integrable) singularity in F_1 is obviously not a problem as far as producing divergent terms is concerned, but for numerical implementation it is clearly beneficial to integrate this singularity analytically. For F_0, however, the behavior is $1/\rho_L$ and is capable of producing a $\log(\,\epsilon\,)$ contribution upon integration. In the following we therefore consider only $m = 0$; $m = 1$ is handled similarly. Note that the dependence of the integrand on θ is harmless; it is $\xi = 0$ which must be dealt with analytically. The needed interchange in the order of integrations is impeded by the fact that Θ_1 and Θ_2 depend on η and ξ. To maneuver around this, introduce the variable t, $-1 \le t \le 1$, via

$$\begin{aligned} \theta &= -\frac{\pi}{2} + \tan^{-1}\left(\frac{t-\eta}{\xi}\right)\ , \\ \frac{d\theta}{dt} &= \frac{\xi}{\xi^2 + (t-\eta)^2}\ , \end{aligned} \tag{24}$$

which also results in $\rho_L = (\xi^2 + (t-\eta)^2)^{1/2}$. As indicated in Figure 1, t is the "end-point" $(t,0)$ of ρ on the ξ^*-axis.

Interchanging the order of integration, (19), for $m = 0$, becomes

$$\frac{J_P^2}{4\pi}\int_{-1}^{1}\mathrm{d}\eta\int_{-1}^{1}\mathrm{d}t\int_0^{\sqrt{3}(1-|\eta|)} \psi_k(\eta,\xi)\,c_{j,0}\,F_0\,\mathrm{d}\xi\ . \tag{25}$$

From (24), the singularity in (20) is now at $t = \eta$, $\xi = 0$, and this once again suggests polar coordinates $\{\Lambda,\Psi\}$ to replace $\{t,\xi\}$,

$$\begin{aligned} t &= \Lambda\cos(\Psi) + \eta\ , \\ \xi &= \Lambda\sin(\Psi)\ , \end{aligned} \tag{26}$$

and integrating with respect to Λ. It is important to note that with the two changes of variables, $\theta \to t$ and $\{t,\xi\} \to \{\Lambda,\Psi\}$, $\cos(\theta)$ becomes $\cos(\Psi)$ and $\sin(\theta)$ becomes $-\sin(\Psi)$. Thus, $a(\theta)$, equation (17), becomes simply $a(\Psi)$ and is a constant as far as the Λ integration is concerned. As shown in Figure 2, the $\{t,\xi\}$ domain is a rectangle,

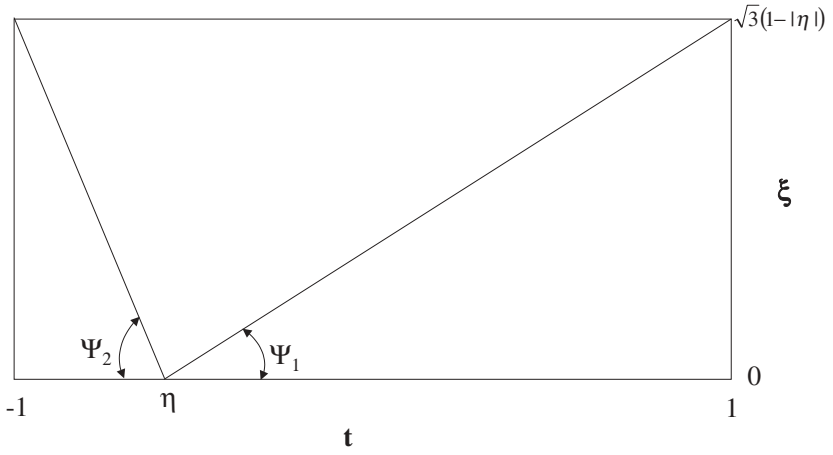

FIG. 2. *Geometry of the second polar coordinate transformation,* $\{t, \xi\} \rightarrow \{\Lambda, \Psi\}$*, for the coincident integration.*

and integrating over $\{\Lambda, \Psi\}$ will necessitate a decomposition into three subdomains $0 \leq \Psi \leq \Psi_1$, $\Psi_1 \leq \Psi \leq \pi - \Psi_2$, and $\pi - \Psi_2 \leq \Psi \leq \pi$, where

$$\Psi_1 = \tan^{-1}\left(\frac{\sqrt{3}(1-|\eta|)}{1-\eta}\right),$$
$$\Psi_2 = \tan^{-1}\left(\frac{\sqrt{3}(1-|\eta|)}{1+\eta}\right). \tag{27}$$

With this final coordinate transformation, the P shape functions are linear in Λ, as are the coefficients $c_{j,m}$ from the Q shape functions. The product is quadratic, and the integrals to be evaluated are therefore of the form

$$-\frac{J_P^2}{4\pi}\int_{-1}^{1} \mathrm{d}\eta \int \sin(\Psi)\,\mathrm{d}\Psi \int_0 \Lambda^s \,\frac{\Lambda^2}{\left(\epsilon^2 + a^2\,\Lambda^2\right)^{3/2}}\,\mathrm{d}\Lambda \tag{28}$$

for $s = 0, 1, 2$. The missing limits for the Λ and Ψ integrals depend upon the particular subtriangle in Figure 2 being considered. Clearly, the Λ integration is trivial, as is, with the exception of $s = 0$, the limit $\epsilon \rightarrow 0$. For $s = 0$ we find a finite contribution plus divergent terms

$$L^c_{kj} = \log(\epsilon)\,\frac{J_P^2}{4\pi}\int_{-1}^{1} \hat{\psi}^0_k\,\hat{\psi}^0_j\,\mathrm{d}\eta \int_0^{\pi} \frac{\sin(\Psi)}{a^3}\,\mathrm{d}\Psi\ , \tag{29}$$

where $\hat{\psi}^0_l$ are the shape functions evaluated at $\Lambda = \rho = 0$, the same for both P and Q:

$$\hat{\psi}^0_1 = \frac{1-\eta}{2}, \qquad \hat{\psi}^0_2 = \frac{1+\eta}{2}, \qquad \hat{\psi}^0_3 = 0\ . \tag{30}$$

As expected, there are no $\log(\epsilon)$ terms associated with ψ_3, as this shape function is zero along the $\xi = 0$ edge; this will of course cycle appropriately when the other

two subtriangles for the Q integration are considered. Note too that as $a = a(\Psi)$ is independent of η, (29) simplifies to

$$L^c_{kj} = \log(\epsilon)\,\frac{J_P^2}{4\pi}\,\frac{1+\delta_{kj}}{3}\int_0^\pi \frac{\sin(\Psi)}{a^3}\,\mathrm{d}\Psi\ , \tag{31}$$

where δ_{kj} is the usual Kronecker delta function and $1 \le k, j \le 2$. We postpone a further discussion of this term until section 6, following the analysis of the edge- and vertex-adjacent integrals. It will be shown that L^c_{kj} cancels with corresponding terms from the edge-adjacent integration. Thus, the desired goal has been achieved: the coincident integral has been separated into a finite, easily evaluated component, plus the divergent term which will be seen to cancel with the adjacent edge integral.

4. Edge-adjacent integration. The treatment of the adjacent edge integral will omit much of the detail, focusing only on the derivation of the divergent term. However, it is instructive to take some space to point out what *does not work*, or at least what does not work very well. In [18], the (simplified) edge-adjacent integral was, as with the coincident case, treated using two analytic integrations. For the general situation, it is possible to push through this analysis, but it leads to extremely complicated and lengthy expressions (in fact, Maple's answers for the analytic integrations contain inverse hyperbolic tangents of complex quantities). The numerical implementation would therefore be inefficient and cumbersome. Moreover, if the Laplace equation produces ugly expressions, the analysis for elasticity would likely be unbearable. The only benefit of pursuing this approach is that the expression for the divergent term involves a single integral instead of the double integral (41) found below. However, it is better to face the nasty integrals once in the proof of cancellation, rather than having to continually compute with them.

The root of the problem is that the expression for the distance r^2 is sufficiently complicated that the double integration is quite involved. To be more specific, orient the elements so that the shared edge is defined by $\xi = 0$ in E_P, and $\xi^* = 0$ for E_Q, and the singularity occurs when $\eta = -\eta^*$. Based upon the successful coincident scheme, a seemingly reasonable approach is to employ polar coordinates for the Q integration,

$$\begin{aligned} \eta^* &= \rho\cos(\theta) - \eta, \\ \xi^* &= \rho\sin(\theta), \end{aligned} \tag{32}$$

and then integrate ρ and ξ analytically. The distance function takes the form

$$r^2 = \epsilon^2 + b_{00}\xi^2 + (b_{10}\epsilon + b_{11}\xi)\rho + b_{22}\rho^2\ , \tag{33}$$

and it is the (unavoidable) presence of the first order term in ρ that creates the complications. The expression obtained by integrating out ρ will have complicated denominators, involving two quadratic factors, one having an integer exponent and one having a half-integer exponent. Thus, the second analytic integration, while possible, results in very lengthy formulas. A different path for the edge integration will therefore be taken, although it will be necessary to confront these types of integrals in the proof that the singularities cancel; see section 6.

A much simpler algorithm, requiring only one analytic integration, begins with the polar coordinates in (32). As shown in Figure 3(a), the θ integration must be split into two pieces (for simplicity, the integrands are omitted, but it will be useful

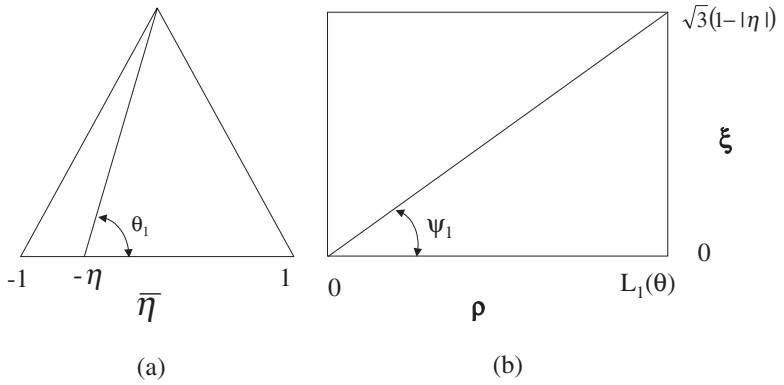

FIG. 3. (a) *Polar coordinate transformation employed in the Q element,* $\{\eta^*, \xi^*\} \rightarrow \{\rho, \theta\}$. (b) *Second polar coordinate transformation* $\{\rho, \xi\} \rightarrow \{\Lambda, \Psi\}$ *for the edge-adjacent integration.*

to retain the Jacobians of the transformations),

$$\int_{-1}^{1} \mathrm{d}\eta \int_{0}^{\sqrt{3}(1-|\eta|)} \mathrm{d}\xi \left[\int_{0}^{\Theta_1(\eta)} \mathrm{d}\theta \int_{0}^{L_+} \rho \, \mathrm{d}\rho + \int_{\Theta_1(\eta)}^{\pi} \mathrm{d}\theta \int_{0}^{L_-} \rho \, \mathrm{d}\rho \right] , \tag{34}$$

where $L^{\pm} = \sqrt{3}(1 \pm \eta)/(\sin(\theta) \pm \sqrt{3}\cos(\theta))$. The key observation is that the breakpoint in θ,

$$\Theta_1(\eta) = \frac{\pi}{2} - \tan^{-1}\left(\frac{\eta}{\sqrt{3}}\right), \tag{35}$$

is only a function of η. The integrations can therefore be rearranged,

$$\begin{aligned} \int_{-1}^{1} \mathrm{d}\eta \int_{0}^{\Theta_1(\eta)} \mathrm{d}\theta \int_{0}^{\sqrt{3}(1-|\eta|)} \mathrm{d}\xi \int_{0}^{L_+} \rho \, \mathrm{d}\rho \\ + \int_{-1}^{1} \mathrm{d}\eta \int_{\Theta_1(\eta)}^{\pi} \mathrm{d}\theta \int_{0}^{\sqrt{3}(1-|\eta|)} \mathrm{d}\xi \int_{0}^{L_-} \rho \, \mathrm{d}\rho \, . \end{aligned} \tag{36}$$

As the singularity occurs when $\rho = \xi = 0$, it makes sense to now introduce a second polar coordinate transformation,

$$\begin{aligned} \rho &= \Lambda \cos(\Psi), \\ \xi &= \Lambda \sin(\Psi). \end{aligned} \tag{37}$$

As $\Lambda = 0$ encapsulates all three conditions for $r = 0$, namely, $\xi = \xi^* = 0$, $\eta = -\eta^*$, one analytic integration (over Λ) will suffice to produce the $\log(\epsilon)$ term. Said another way, the combined Jacobian from the two transformations is $\cos(\Psi)\Lambda^2$, and the Λ^2 factor from the two polar transformations sufficiently reduces the order of the singularity that only the constant ($\Lambda = 0$) term from the product of the shape functions poses any difficulty. As in the coincident algorithm, the exact integration is with respect to the distance from the singularity. Moreover, both algorithms indicate that in order to fully attend to the singularity, both inner and outer integrations must be involved.

The second point to note is that although distance takes the form

$$r^2 = \epsilon^2 - \epsilon b_1 \Lambda + b_2 \Lambda^2 \, , \tag{38}$$

the first order term in Λ does not present a major problem: there is only one integration, and, moreover, the ϵ factor will eventually simplify the resulting expressions.

Carrying out the Λ integration results in a finite quantity plus a divergent contribution,

$$L^e_{kj} = \log(\epsilon)\,\frac{1}{4\pi}\int_{-1}^{1}\hat{\psi}^0_k\,\hat{\psi}^0_j\,\mathrm{d}\eta\int_0^{\pi}\mathrm{d}\theta\int_0^{\pi/2}\cos(\Psi)\left(\frac{3j_{1p}j_{1q}}{b_2^{5/2}}-\frac{\mathbf{n}\bullet\mathbf{N}}{b_2^{3/2}}\right)\mathrm{d}\Psi\ , \tag{39}$$

where j_{1p} and j_{1q} are the coefficients of Λ in $J_Q\mathbf{n}\bullet\mathbf{R}$ and $J_P\mathbf{N}\bullet\mathbf{R}$,

$$\begin{aligned} J_P\mathbf{N}\bullet\mathbf{R} &= j_{1p}\Lambda - J_P\epsilon,\\ J_Q\mathbf{n}\bullet\mathbf{R} &= j_{1q}\Lambda - J_Q\mathbf{n}\bullet\mathbf{N}\ . \end{aligned} \tag{40}$$

As in (29), $\hat{\psi}^0_k$ and $\hat{\psi}^0_j$ denote the shape functions evaluated at $\Lambda = 0$. Here we have a slight problem with notation in matching the edge L^e_{kj} terms with the coincident L^c_{kj}. In the edge ordering, node 1 in P is node 2 in Q and vice versa. Thus, L^e_{11} corresponds to the off-diagonal contribution L^c_{12}, and L^e_{12} should cancel with L^c_{11}. To simplify the discussion of the cancellation, we adopt, for (39), the convention that the subscripts refer to the coincident integral (i.e., the numbering of the P element). In this case, $\hat{\psi}^0_l$ are the same for P and Q and, moreover, given by (30). It is important to note that b_2 is a function of the nodal coordinates and the angles θ, Ψ, but not of η, and indeed all other quantities in the integrand are independent of η. Thus, (39) reduces to

$$L^e_{kj} = \log(\epsilon)\,\frac{1}{4\pi}\,\frac{1+\delta_{kj}}{3}\int_0^{\pi}\mathrm{d}\theta\int_0^{\pi/2}\cos(\Psi)\left(\frac{3j_{1p}j_{1q}}{b_2^{5/2}}-\frac{\mathbf{n}\bullet\mathbf{N}}{b_2^{3/2}}\right)\mathrm{d}\Psi\ , \tag{41}$$

again for $1 \le k, j \le 2$. This expression and that for L^c_{kj}, (31), do not, at first sight, appear to cancel. The proof that they do will be given in section 6 following a discussion of the vertex integration.

5. Vertex-adjacent integration. As discussed above, the vertex-adjacent integrals are separately finite, the singularity being limited to a single point in the four-dimensional integration. Thus, any number of different algorithms can be used to evaluate these terms. However, the procedures described above, when suitably modified for the vertex situation, will integrate the singularity as completely as possible using one analytic integration, and would therefore appear to be an effective and efficient approach. The discussion that follows will simply outline the basic procedure, highlighting only the differences from the edge-adjacent case.

Orient the P and Q elements so that the singular point is $\eta = -1$ and $\eta^* = -1$. Separate polar coordinates can then be introduced in each element,

$$\begin{aligned} \eta^* &= \rho_q\cos(\theta_q) - 1, \qquad \xi^* = \rho_q\sin(\theta_q),\\ \eta &= \rho_p\cos(\theta_p) - 1, \qquad \xi = \rho_p\sin(\theta_p). \end{aligned} \tag{42}$$

This results in an integral of the form (again omitting the kernel function and just keeping track of the Jacobians)

$$\begin{aligned} &\int_0^{\pi/3}\mathrm{d}\theta_p\int_0^{L_p(\theta_p)}\rho_p\,\mathrm{d}\rho_p\int_0^{\pi/3}\mathrm{d}\theta_q\int_0^{L_q(\theta_q)}\rho_q\,\mathrm{d}\rho_q\\ &\qquad = \int_0^{\pi/3}\mathrm{d}\theta_p\int_0^{\pi/3}\mathrm{d}\theta_q\int_0^{L_p(\theta_p)}\rho_p\,\mathrm{d}\rho_p\int_0^{L_q(\theta_q)}\rho_q\,\mathrm{d}\rho_q, \end{aligned} \tag{43}$$

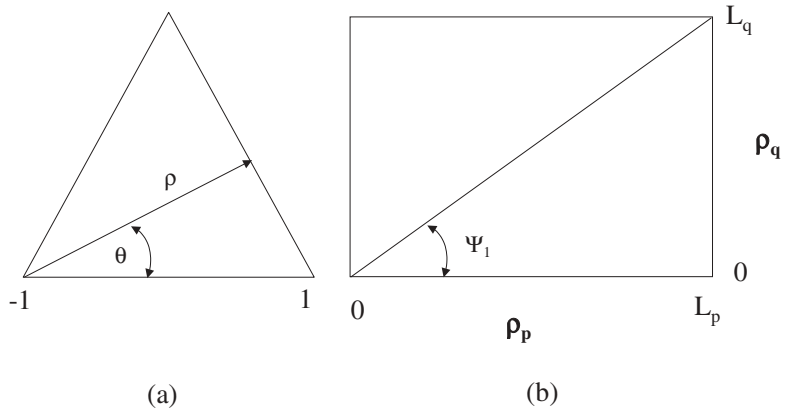

FIG. 4. (a) *Initial polar coordinate transformation employed in both P and Q elements.* (b) *Final polar coordinate transformation* $\{\rho_p, \rho_q\} \to \{\Lambda, \Psi\}$ *for the vertex adjacent integration.*

where $L_p(\theta_p) = 2\sqrt{3}/\left[\sin(\theta_p) + \sqrt{3}\cos(\theta_p)\right]$, and similarly for L_q. The lone singularity is at the common vertex $\rho_p = \rho_q = 0$, and thus one further polar coordinate transformation,

$$\begin{aligned} \rho_p &= \Lambda\cos(\Psi), \\ \rho_q &= \Lambda\sin(\Psi), \end{aligned} \tag{44}$$

is warranted. As indicated in Figure 4, the $\{\rho_p, \rho_q\}$ domain is a rectangle, and thus the Ψ integration must be taken in two pieces. The combined Jacobian in this case is $\cos(\Psi)\sin(\Psi)\Lambda^3$, and thus (43) becomes

$$\begin{aligned} \int_0^{\pi/3} \mathrm{d}\theta_p \int_0^{\pi/3} \mathrm{d}\theta_q \Bigg[\int_0^{\Psi_1} \cos(\Psi)\sin(\Psi)\,\mathrm{d}\Psi \int_0^{L_1(\Psi)} \Lambda^3\,\mathrm{d}\Lambda \\ + \int_{\Psi_1}^{\pi/2} \cos(\Psi)\sin(\Psi)\,\mathrm{d}\Psi \int_0^{L_2(\Psi)} \Lambda^3\,\mathrm{d}\Lambda \Bigg] , \end{aligned} \tag{45}$$

where $L_1(\Psi) = L_P(\theta_p)/\cos(\Psi)$ and $L_2(\Psi) = L_Q(\theta_q)/\sin(\Psi)$. With the Λ^3 factor the kernel function simplifies, as it is possible to immediately set $\epsilon = 0$, and the distance is then $r^2 = b^2\Lambda^2$ (the coefficient being a function of all three angles and nodal coordinates). Thus, it is then apparent that this integral is finite, and it is a simple matter to execute the analytic integrations.

6. Proof of cancellation. Recapitulating the above results, the coincident and edge-adjacent integrations give rise to divergent $\log(\epsilon)$ terms of the form

$$\begin{aligned} L^c_{kj} &= \frac{J_P^2}{4\pi}\,\frac{1+\delta_{kj}}{3}\int_0^{\pi}\frac{\sin(\Psi)}{a^3}\,\mathrm{d}\Psi, \\ L^e_{kj} &= \frac{1}{4\pi}\,\frac{1+\delta_{kj}}{3}\int_0^{\pi}\mathrm{d}\theta\int_0^{\pi/2}\cos(\Psi)\left(\frac{3j_{1p}j_{1q}}{b_2^{5/2}} - \frac{\mathbf{n}\bullet\mathbf{N}}{b_2^{3/2}}\right)\mathrm{d}\Psi\ , \end{aligned} \tag{46}$$

where $k, j = 1, 2$ refer to the two nodes P_1 and P_2 along the common edge. It is therefore necessary to establish that

$$J_P^2 \int_0^\pi \frac{\sin(\Psi)}{a^3}\,\mathrm{d}\Psi = -\int_0^\pi \mathrm{d}\theta \int_0^{\pi/2} \cos(\Psi)\left(\frac{3 j_{1p} j_{1q}}{b_2^{5/2}} - \frac{\mathbf{n}\bullet\mathbf{N}}{b_2^{3/2}}\right)\mathrm{d}\Psi\ , \tag{47}$$

and this will be accomplished by brute force, evaluating the integrals. This is most easily carried out using a symbolic computation program.

To simplify matters, it is convenient (and permissible) to shift and rotate the elements so that $P_1 = (0,0,0)$, $P_2 = (x_2, 0, 0)$, and $P_3 = (x_3, y_3, 0)$, and thus $\mathbf{N} = (0,0,1)$ and $J_P = x_2 y_3 / 2\sqrt{3}$. Note that for the edge-adjacent Q-element, the convention is that $Q_1 = P_2$ and $Q_2 = P_1$. Denoting the coordinates of Q_3 by $Q_3 = (x_3^*, y_3^*, z_3^*)$, the normal for Q is $J_Q \mathbf{n} = (0,\ z_3^* x_2,\ -y_3^* x_2)$.

From (17) and the comment below (26), the divergent term for the coincident integral takes the form

$$J_P^2 \int_0^\pi \frac{\sin(\Psi)}{\left(\, a_{cc}\cos(\Psi)^2 - a_{cs}\cos(\Psi)\sin(\Psi) + a_{ss}\sin(\Psi)^2 \,\right)^{3/2}}\,\mathrm{d}\Psi\ , \tag{48}$$

and for the shifted geometry,

$$a_{cc} = \frac{1}{4}\, x_2^2, \tag{49}$$

$$a_{cs} = \sqrt{3}\, x_2\,(2\, x_3 - x_2)\,/6, \tag{50}$$

$$a_{ss} = \left(\, x_2^2 + 4\, x_3^2 + 4\, y_3^2 - 4\, x_3\, x_2 \,\right)/12.$$

After substituting $q = \operatorname{cotan}(\Psi)$, (48) becomes

$$-J_P^2 \int_{-\infty}^{\infty} \frac{1}{\left(\, a_{cc} q^2 - a_{cs} q + a_{ss} \,\right)^{3/2}}\,\mathrm{d}q\ , \tag{51}$$

and carrying out the integration, we find that the coincident divergent term becomes simply

$$J_P^2 \int_0^\pi \frac{\sin(\Psi)}{a^3}\,\mathrm{d}\Psi = x_2\ . \tag{52}$$

Thus, as expected, the divergent term does not depend upon P_3.

The evaluation of the edge integral divergent term is somewhat more involved. Although symbolic computation will eventually execute all of the required calculus and algebra, some manipulation is required to modify the forms of the expressions, and care is required to keep the size of the expressions from exceeding the available memory. The discussion below will therefore only outline the procedure. As a function of Ψ, the coefficient b_2 defined in (38) takes the form

$$b_2 = c_2 \cos^2(\Psi) + c_1 \cos(\Psi)\sin(\Psi) + c_0 \sin^2(\Psi), \tag{53}$$

where the c_j are functions of $\cos(\theta)$ and $\sin(\theta)$. Thus, as with L_{kj}^c, substituting $q = \operatorname{cotan}(\Psi)$ is convenient, resulting in an integral of the form

$$\int_0^\infty \left[\, \alpha_1 \frac{q^2}{\left(\, c_2 q^2 + c_1 q + c_0 \,\right)^{5/2}} + \alpha_2 \frac{q}{\left(\, c_2 q^2 + c_1 q + c_0 \,\right)^{3/2}} \,\right] \mathrm{d}q\ . \tag{54}$$

The function of θ that results from this integration once again benefits from the substitution $p = \text{cotan}(\theta)$, and the θ integral becomes

$$\int_{-\infty}^{\infty} \frac{h_1(p)}{(\, s_2p^2 + s_1p + s_0\,)^2}\,\mathrm{d}p + \int_{-\infty}^{\infty} \frac{h_2(p)}{\sqrt{(t_2p^2 + t_1p + t_0)}\,(\, s_2p^2 + s_1p + s_0\,)^2}\,\mathrm{d}p\ , \tag{55}$$

where $h_1(p)$ and $h_2(p)$ are quadratic and cubic polynomials, respectively. The coefficients $\{s_j\}$ and $\{t_j\}$ are now just functions of the nodal coordinates. The first integral is found to be 0, while the second is, as desired, $-x_2$.

7. Test calculations. To confirm that the above procedures are successful, results obtained using the symmetric-Galerkin approximation are presented in this section. The first two calculations are relatively simple standard test problems having known analytic solutions. The first is a mixed boundary value problem on the unit cube, and the second is a pressurized penny-shaped crack in an infinite medium. The third example is a thermal analysis in a nonhomogeneous medium, a functionally graded material. The purpose of this example is to demonstrate the singular integration techniques for a hypersingular kernel that is substantially more complicated than that for the Laplace equation. In symmetric-Galerkin, the hypersingular flux equation is employed on the Neumann surface (the equation for surface potential, (4), is used on the Dirichlet surface), so all problems will have boundary data specifying the normal derivative.

All singular integrals in (4) and (7) are computed using the algorithms described herein. For the singular integration, the parameter space integrals that remain after the analytic integration are evaluated using a one-dimensional twelve-point Gauss quadrature formula. The nonsingular integrals are computed using a two-dimensional twelve-point Gauss rule for the equilateral triangle.

7.1. Unit cube. The purpose of the unit cube, $0 \le x, y, z \le 1$, example is to test the adjacent edge and vertex algorithms in situations where the adjacent elements are far from being coplanar. The boundary conditions on $x = 0$ and $x = 1$ were values for potential, and the flux was specified on the remaining faces. The values were taken as the boundary potential and flux from the harmonic function $\phi(x, y, z) = x^2 + y^2 - 2z^2$, so the exact solution is known. The cube was uniformly discretized using M elements, for various values of M. As noted above, the hypersingular equation is employed on the Neumann surface, and thus these equations are associated with the unknown potentials.

Figure 5 plots the maximum absolute error in the computed surface potential as a function of M. For comparison purposes, the maximum error obtained by solving the problem by means of the potential equation alone is also displayed. The improved accuracy with symmetric-Galerkin is possibly due to the fact that the kernel functions die off faster with increasing r; as a consequence, the singular integrations (evaluated partly analytically) in this calculation are more influential than those for the potential equation.

7.2. Pressurized crack. As one of the main applications of hypersingular equations is fracture analysis [5, 7, 58], the second test case is a simple crack problem. The geometry is a "penny-shaped" crack $x^2 + y^2 \le R_0 = \sqrt{2}/10$, $z = 0$, embedded in an infinite medium, with boundary condition $[\,\partial\phi/\partial\mathbf{n}\,] = 1$. The square bracket notation denotes the sum of the fluxes,

$$\left[\,\frac{\partial\phi}{\partial\mathbf{n}}\,\right](P) = \frac{\partial\phi}{\partial\mathbf{n}}(P^+) + \frac{\partial\phi}{\partial\mathbf{n}}(P^-)\ , \tag{56}$$

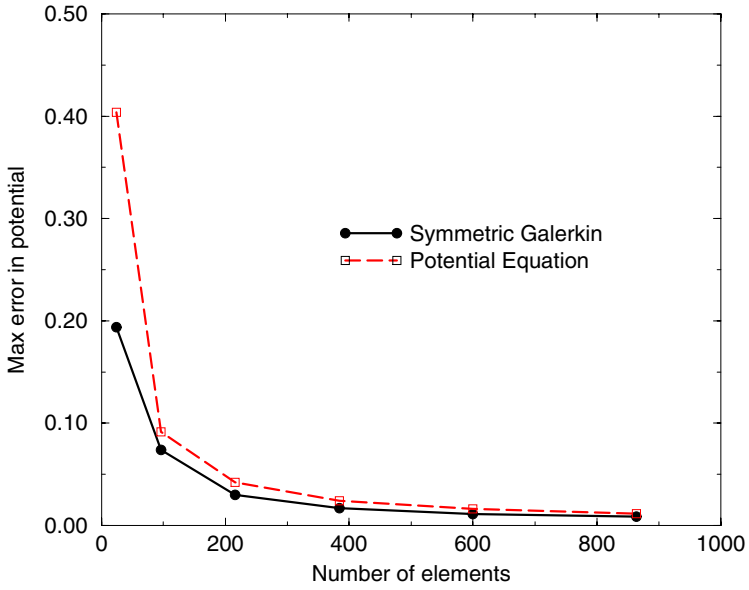

FIG. 5. *The maximum absolute error in the computed potential is plotted as a function of the number of elements discretizing the unit cube.*

where P^+ and P^- are at the same location but on opposite sides of the crack. The quantity to be determined is the jump in potential across the crack

$$[\,\phi\,](P) = \phi(P^+) - \phi(P^-)\ , \tag{57}$$

and setting $r^2 = x^2 + y^2$, the exact solution is [35, p. 144]

$$[\phi]\,(x,y) = \frac{2R_0}{\pi}\left(1 - \frac{r^2}{R_0^2}\right)^{1/2}\ . \tag{58}$$

The crack was discretized with 214 nodes and 382 elements, but *without* a special crack tip element [2, 28, 52] to capture the $\sqrt{R_0^2 - r^2}$ behavior at $r = R_0$. Thus error near the crack front is to be expected. The exact jump in potential from (58) is plotted against the computed solution in Figure 6. Although the inappropriate linear element at the front causes some error, this solution is generally quite accurate.

7.3. Graded material. As mentioned in the introduction, one motivation for pursuing a direct method is that this approach is expected to be applicable to any boundary integral formulation, i.e., any Green's function. To bolster this contention and, moreover, to present a calculation in an area of significant current interest in materials science and engineering [48], a thermal analysis in a functionally graded material (FGM) is briefly described below. More complete details about the boundary integral implementation for this application can be found in [61].

The Laplace equation for a general thermal conductivity $\kappa(x,y,z)$ is

$$\nabla\bullet(\kappa\nabla\phi) = 0\ . \tag{59}$$

In an FGM, the grading is most often only in one direction, and generally modeled as

$$\kappa(x,y,z) = \kappa(z) = \kappa_0 e^{2\beta z}\ , \tag{60}$$

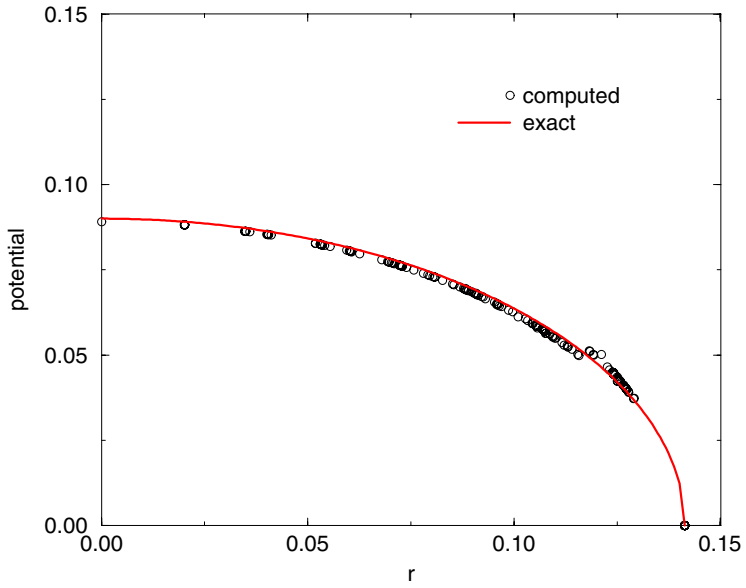

FIG. 6. *The solution for* $[\phi]$ *for the pressurized penny-shaped crack;* r *is the distance from the center of the disk.*

where β denotes the material grading parameter. The Green's function for this exponential grading has been derived [19, 36],

$$G(P,Q) = \frac{e^{\beta(-r+R_z)}}{4\pi r} \tag{61}$$

($R_z = Q_z - P_z$ is the z-coordinate of $Q - P$), and the governing (interior limit) boundary integral equation is

$$\phi(P) + \int_\Sigma \left[\phi(Q) \left(\frac{\partial}{\partial n} G(P,Q) - 2\beta n_z G(P,Q) \right) - G(P,Q) \frac{\partial}{\partial n} \phi(Q) \right] \mathrm{d}Q = 0 \ . \tag{62}$$

Note, however, that $G(P,Q)$ is not a symmetric function of Q and P, and this precludes a symmetric-Galerkin implementation. As discussed in [61], this can be remedied by writing (62) in terms of the surface flux, $-\kappa(Q)\frac{\partial}{\partial n}\phi(Q)$, rather than the normal derivative. The appropriate symmetric Green's function is then

$$G_S(P,Q) = -\frac{G(P,Q)}{\kappa(z_Q)} = -\frac{1}{4\kappa_0 \pi} \frac{e^{\beta(-r-Q_z-P_z)}}{r} \ . \tag{63}$$

The corresponding integral equation for surface flux is obtained by differentiating (62) in the direction $\mathbf{N}$, and then multiplying by $-\kappa(z_P)$. The hypersingular kernel function that results is given by the lengthy expression

$$\begin{aligned} \frac{\kappa_0}{4\pi} e^{\beta(-r+Q_z+P_z)} \Bigg(& 3\frac{(\mathbf{n}\bullet\mathbf{R})(\mathbf{N}\bullet\mathbf{R})}{r^5} + 3\beta\frac{(\mathbf{n}\bullet\mathbf{R})(\mathbf{N}\bullet\mathbf{R})}{r^4} \\ & + \frac{\beta^2(\mathbf{n}\bullet\mathbf{R})(\mathbf{N}\bullet\mathbf{R}) - \beta(N_z\mathbf{n} - n_z\mathbf{N})\bullet\mathbf{R} - \mathbf{n}\bullet\mathbf{N}}{r^3} \\ & - \beta\frac{\beta(N_z\mathbf{n} - n_z\mathbf{N})\bullet\mathbf{R} + \mathbf{n}\bullet\mathbf{N}}{r^2} - \beta^2\frac{N_z n_z}{r} \Bigg) \ . \end{aligned} \tag{64}$$

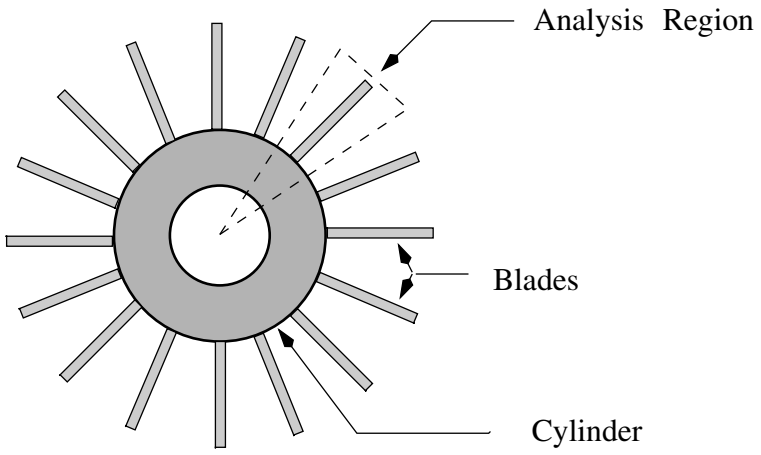

FIG. 7. *Top view of the compressor blade assembly.*

A Stokes formulation for the Galerkin integral of this function is likely to be possible, but equally likely to be quite complicated. The boundary limit formulation applies with almost no change, the only new aspect being the use of simple one- and two-term Taylor expansions to handle the exponential factor [61]. The analytic integrations and limit will obviously involve lengthier expressions, but otherwise the analysis is basically no more complicated than for $\beta = 0$. Moreover, it is possible to automate this work using symbolic computation. Thus, the evaluation of the Galerkin integral of (64), while not entirely trivial, does proceed in a straightforward fashion.

As an example, a symmetric Galerkin analysis of a graded compressor has been carried out. A top view of the full geometry is shown in Figure 7, while the symmetric section employed in the calculation is shown in Figure 8. The rotor blade is graded in the z-coordinate, which is the vertical direction in this latter figure. The grading is given by (60) with $\kappa_0 = 5$ and $\beta = 0.25$,

$$\kappa(z) = 5e^{z/2}. \tag{65}$$

To have an analytic solution (for comparison purposes) for this somewhat complicated geometry, the boundary conditions have been chosen to reduce the problem to a one-dimensional solution (the goal herein is simply to demonstrate that the hypersingular implementation is correct). As shown in Figure 8, the temperatures at the top $z = 3$ and bottom $z = 0$ are held at $\phi = 200$ and $\phi = 100$, respectively. The remaining surfaces are insulated (zero flux), and consequently the hypersingular flux equation is employed everywhere except on the top and bottom. The exact solution for this problem is, with $L = 3$, given by

$$\phi = 100 + 100\frac{1 - e^{-2\beta z}}{1 - e^{-2\beta L}}. \tag{66}$$

As noted above, the solution at corners and edges generally provides a good indication of whether or not the numerical implementation is correct. Figure 9 plots the analytic and computed solutions for temperature along the edge labeled $[AA]$ in Figure 8, and the results are reasonably good. The computed fluxes on $z = 0$ and $z = 3$ are also accurate: the exact values are, respectively, ± 321.8, while the calculated values are ± 322.8.

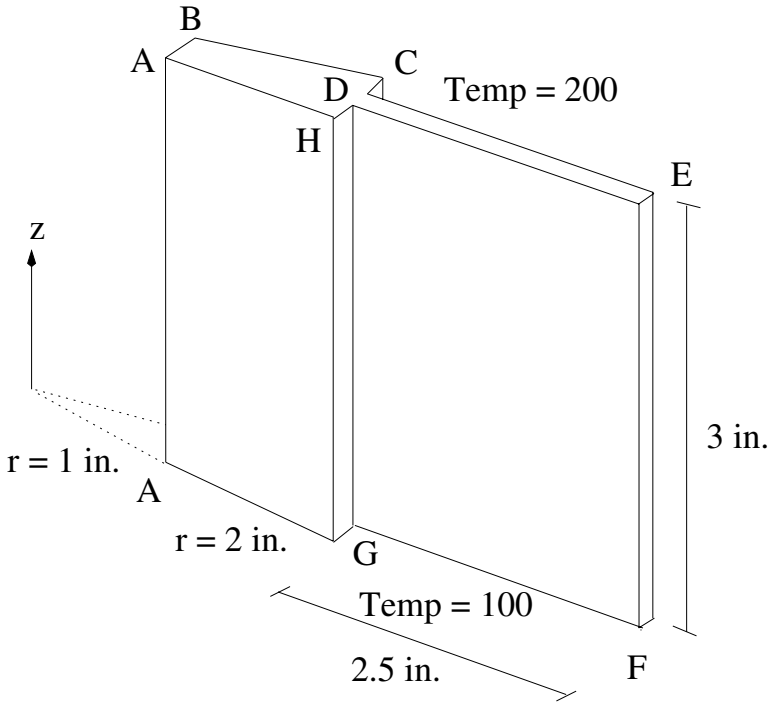

FIG. 8. *Section of the blade assembly that has been modeled.*

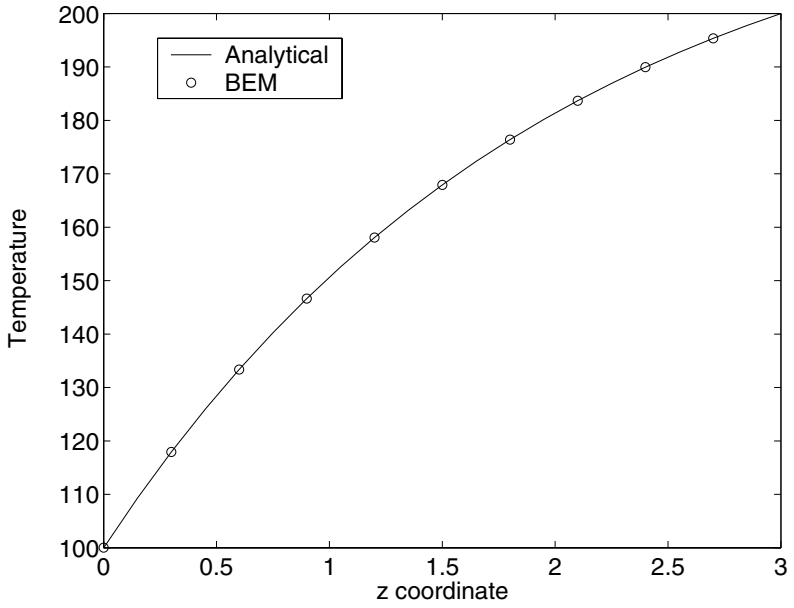

FIG. 9. *Analytical and numerical solutions for the temperature along a vertical edge of the blade assembly.*

8. Conclusions. Procedures for directly evaluating Galerkin hypersingular (and singular) integrals have been presented. For the coincident and edge-adjacent cases, the key is to explicitly identify the divergent terms that appear in the limit to the boundary. To this end, multiple polar coordinate transformations and analytic integration were employed. This results in an efficient scheme, as the remaining, reduced dimension, numerical integration involves only smooth functions. Although the coincident and adjacent-edge integrals were shown to be separately divergent, as expected, the $\log(\epsilon)$ terms cancel when all integrals are added.

As discussed in detail elsewhere [22], a principal benefit of the limit definition of the hypersingular integral is that it leads to an efficient Galerkin algorithm for computing tangential derivatives (e.g., $\nabla\phi$) on the boundary. This postprocessing task is generally required to compute surface velocities when simulating moving boundaries, a class of problems for which integral equation methods should be advantageous.

Although the simplest situation—the Laplace Green's function and a linear element approximation—was considered, a second important aspect of this approach is that it should be generally applicable. As evidence of this, a calculation involving the Green's function for an exponentially graded material was presented; a complete discussion can be found in [61]. In addition, progress towards implementing this approach for three-dimensional anisotropic elasticity is discussed in [17].

Fracture analysis is an important application of hypersingular equations, and for this work it is essential to employ higher order elements. The two main complications not present in the linear element analysis are that the distance function is no longer quadratic, as in (19) or (16), and that the normal vectors and Jacobians are no longer constants over the elements. This precludes an analytic integration of the complete integrands as carried out above. As with more complicated Green's functions (see, for example, [17]), it will be necessary to split the integrals into two parts: one that contains all of the singularity but is sufficiently simplified that analytic evaluation is possible, plus a remainder that is well-behaved and can be treated entirely numerically. This can be accomplished using techniques that are similar to those employed for two-dimensional problems [16]. However, these methods must be modified somewhat for three dimensions: the powers of the quadratics that will appear in the denominators are now half-integers instead of integers, and this necessitates some changes to the procedures for splitting the integrand into singular and nonsingular components. These needed modifications will be described in a separate publication.

Acknowledgments. The authors are indebted to G. Maier, A. Frangi, and S. Salvadori for useful discussions, to S. Salvadori for a preprint in advance of publication, and to A. Sutradhar for the graded material calculation presented herein.

REFERENCES

[1] A. Aimi and M. Diligenti, *Hypersingular kernel integration in 3D Galerkin boundary element method*, J. Comput. Appl. Math., 138 (2002), pp. 51–72.

[2] R. S. Barsoum, *On the use of isoparametric finite elements in linear fracture mechanics*, Internat. J. Numer. Methods Engrg., 10 (1976), pp. 25–37.

[3] J. R. Berger, P. A. Martin, V. Mantic, and L. J. Gray, *An anisotropic 2-dimensional fundamental solution for steady-state heat transfer*, Z. Angew. Math. Phys, to appear.

[4] M. Bonnet, *Boundary Integral Equation Methods for Solids and Fluids*, Wiley, Chichester, UK, 1995.

[5] M. Bonnet and H. D. Bui, *Regular BIE for three-dimensional cracks in elastodynamics*, in Advanced Boundary Element Methods, T. A. Cruse, ed., Springer-Verlag, Berlin, New York, 1988, pp. 41–47.

[6] M. Bonnet, G. Maier, and C. Polizzotto, *Symmetric Galerkin boundary element method*, ASME Appl. Mech. Rev., 51 (1998), pp. 669–704.
[7] H. D. Bui, *An integral equation method for solving the problem of a plane crack of arbitrary shape*, J. Mech. Phys. Solids, 25 (1977), pp. 29–39.
[8] A. Carini, M. Diligenti, P. Maranesi, and M. Zanella, *Analytical integrations for two dimensional elastic analysis by the symmetric Galerkin boundary element method*, Comput. Mech., 23 (1999), pp. 308–323.
[9] A. Carini and A. Salvadori, *Analytical integrations* 3*D BEM*, Comput. Mech., 28 (2002), pp. 177–185.
[10] T. A. Cruse and J. D. Richardson, *Non-singular Somigliana stress identities in elasticity*, Internat. J. Numer. Methods Engrg., 39 (1996), pp. 3273–3304.
[11] V. J. Ervin and E. P. Stephan, *A boundary element Galerkin method for a hypersingular integral equation on open surfaces*, Math. Methods Appl. Sci., 13 (1990), pp. 281–289.
[12] A. Frangi, *Regularization of boundary element formulations by the derivative transfer method*, in Singular Integrals in the Boundary Element Method, V. Sladek and J. Sladek, eds., Advances in Boundary Elements, Computational Mechanics Publications, Southampton, UK, 1998, pp. 125–164.
[13] A. Frangi and G. Novati, *Symmetric BE method in two-dimensional elasticity: Evaluation of double integrals for curved elements*, Comput. Mech., 19 (1996), pp. 58–68.
[14] L. J. Gray, *Boundary element method for regions with thin internal cavities*, Engrg. Anal. Boundary Elem., 6 (1989), pp. 180–184.
[15] L. J. Gray, *Evaluation of hypersingular integrals in the boundary element method*, Math. Comput. Modelling, 15 (1991), pp. 165–174.
[16] L. J. Gray, *Evaluation of singular and hypersingular Galerkin boundary integrals: Direct limits and symbolic computation*, in Singular Integrals in the Boundary Element Method, V. Sladek and J. Sladek, eds., Advances in Boundary Elements, Computational Mechanics Publications, Southampton, UK, 1998, pp. 33–84.
[17] L. J. Gray, A. Griffith, L. Johnson, and P. A. Wawrzynek, *Evaluation of Galerkin singular integrals for anisotropic elasticity: Displacement equation*, Elect. J. Boundary Elements, 1 (2003), pp. 68–94.
[18] L. J. Gray and T. Kaplan, 3*D Galerkin integration without Stokes' theorem*, Engrg. Anal. Boundary Elem., 25 (2001), pp. 289–295.
[19] L. J. Gray, T. Kaplan, J. D. Richardson, and G. H. Paulino, *Green's functions and boundary integral analysis for exponentially graded materials: Heat conduction*, ASME J. Appl. Mech., 70 (2003), pp. 543–549.
[20] L. J. Gray, D. Maroudas, and M. Enmark, *Galerkin boundary integral method for evaluating surface derivatives*, Comput. Mech., 22 (1998), pp. 187–193.
[21] L. J. Gray, L. F. Martha, and A. R. Ingraffea, *Hypersingular integrals in boundary element fracture analysis*, Internat. J. Numer. Methods Engrg., 29 (1990), pp. 1135–1158.
[22] L. J. Gray, A.-V. Phan, and T. Kaplan, *Boundary integral evaluation of surface derivatives*, SIAM J. Sci. Comput., to appear.
[23] S. T. Grilli, P. Guyenne, and F. Dias, *A fully nonlinear model for three-dimensional overturning waves over arbitrary bottom*, Internat. J. Numer. Methods Fluids, 35 (2001), pp. 829–867.
[24] M. Guiggiani, G. Krishnasamy, T. J. Rudolphi, and F. J. Rizzo, *A general algorithm for the numerical solution of hypersingular boundary integral equations*, ASME J. Appl. Mech., 59 (1992), pp. 604–614.
[25] M. R. Gungor, L. J. Gray, and D. Maroudas, *Effects of mechanical stress on electromigration-driven transgranular void dynamics in passivated metallic thin films*, Appl. Phys. Lett., 73 (1998), pp. 3848–3850.
[26] J. Hadamard, *Lectures on Cauchy's Problem in Linear Partial Differential Equations*, Dover, New York, 1952.
[27] F. Hartmann, C. Katz, and B. Protopsaltis, *Boundary elements and symmetry*, Ing.-Arch., 55 (1985), pp. 440–449.
[28] R. D. Henshell and K. G. Shaw, *Crack tip finite elements are unnecessary*, Internat. J. Numer. Methods Engrg., 9 (1975), pp. 495–507.
[29] S. M. Hölzer, *The symmetric Galerkin BEM in elasticity: FEM/BEM coupling, integration and adaptivity*, Comput. Mech., submitted.
[30] S. M. Hölzer, *The symmetric Galerkin BEM for plane elasticity: Scope and applications*, in Numerical Methods in Engineering '92, C. Hirsch, ed., Elsevier, Amsterdam, 1992.
[31] S. M. Hölzer, *How to deal with hypersingular integrals in the symmetric BEM*, Comm. Numer. Methods Engrg., 9 (1993), pp. 219–232.

[32] Q. Huang and T. A. Cruse, *On the nonsingular traction-BIE in elasticity*, Internat. J. Numer. Methods Engrg., 37 (1994), pp. 2041–2072.
[33] N. I. Ioakimidis, *A natural approach to the introduction of finite-part integrals into crack problems of three-dimensional elasticity*, Engrg. Fract. Mech., 16 (1982), pp. 669–673.
[34] N. I. Ioakimidis, *Exact expression for a two-dimensional finite part integral appearing during the numerical solution of crack problems in three-dimensional elasticity*, Comm. Appl. Numer. Methods, 1 (1985), pp. 183–189.
[35] H. Lamb, *Hydrodynamics*, 6th ed., Dover, New York, 1945.
[36] B. Q. Li and J. W. Evans, *Boundary element solution of heat convection-diffusion problems*, J. Comput. Phys., 93 (1991), pp. 255–272.
[37] S. Li, M. E. Mear, and L. Xiao, *Symmetric weak form integral equation method for three-dimensional fracture analysis*, Comput. Methods Appl. Mech. Engrg., 151 (1998), pp. 435–459.
[38] E. D. Lutz, *Singular and Nearly Singular Integrals*, Ph.D. thesis, Cornell University, Ithaca, NY, 1991.
[39] G. Maier, M. Diligenti, and A. Carini, *A variational approach to boundary element elastodynamic analysis and extension to multidomain problems*, Comput. Methods Appl. Engrg., 92 (1991), pp. 193–213.
[40] G. Maier, S. Miccoli, G. Novati, and S. Sirtori, *A Galerkin symmetric boundary element methods in plasticity: Formulation and implementation*, in Advances in Boundary Element Techniques, J. H. Kane, G. Maier, N. Tosaka, and S. N. Atluri, eds., Springer-Verlag, Berlin, Heidelberg, 1993, pp. 288–328.
[41] G. Maier and C. Polizzotto, *A Galerkin approach to boundary element elastoplastic analysis*, Comput. Methods Appl. Mech. Engrg., 60 (1987), pp. 175–194.
[42] S. Maiti, G. H. Paulino, and P. H. Geubelle, *A novel frictionless contact formulation and implementation using the boundary element method*, Internat. J. Numer. Methods Engrg., to appear.
[43] P. A. Martin, *On functionally graded balls and cones*, J. Engrg. Math., 42 (2002), pp. 133–142.
[44] P. A. Martin, J. D. Richardson, L. J. Gray, and J. Berger, *On Green's function for a three-dimensional exponentially-graded elastic solid*, R. Soc. Lond. Proc. Ser. A Math. Phys. Eng. Sci., 48 (2002), pp. 1931–1948.
[45] P. A. Martin and F. J. Rizzo, *On boundary integral equations for crack problems*, Proc. Roy. Soc. London Ser. A, 421 (1989), pp. 341–355.
[46] P. A. Martin and F. J. Rizzo, *Hypersingular integrals: How smooth must the density be?*, Internat. J. Numer. Methods Engrg., 39 (1996), pp. 687–704.
[47] P. A. Martin, F. J. Rizzo, and T. A. Cruse, *Smoothness-relaxation strategies for singular and hypersingular integral equations*, Internat. J. Numer. Methods Engrg., 42 (1998), pp. 885–906.
[48] Y. Miyamoto, W. A. Kaysser, B. H. Rabin, A. Kawasaki, and R. G. Ford, *Functionally Graded Materials: Design, Processing and Applications*, Kluwer Academic, Dordrecht, The Netherlands, 1999.
[49] A. Nagarajan, E. D. Lutz, and S. Mukherjee, *A novel boundary elements method for linear elasticity with no numerical integration for* $2d$ *and line integrals for* $3d$ *problems*, J. Appl. Mech., 61 (1994), pp. 264–269.
[50] A. Nagarajan, E. D. Lutz, and S. Mukherjee, *The boundary contour method for three dimensional linear elasticity*, J. Appl. Mech., 63 (1996), pp. 278–286.
[51] G. H. Paulino and L. J. Gray, *Galerkin residuals for error estimation and adaptivity in the symmetric Galerkin boundary integral method*, ASCE Engrg. Mech., 125 (1999), pp. 575–585.
[52] A.-V. Phan, L. J. Gray, G. H. Paulino, and T. Kaplan, *Improved quarter-point crack tip element*, Engrg. Fract. Mech., 70 (2003), pp. 269–283.
[53] A.-V. Phan, T. Kaplan, L. J. Gray, D. Adelsteinsson, J. A. Sethian, W. Barvosa-Carter, and M. A. Aziz, *Modeling a growth instability in a stressed solid*, Modelling Simulation Mater. Sci. Engrg., 9 (2001), pp. 309–325.
[54] A. Salvadori, *Quasi Brittle Fracture Mechanics by Cohesive Crack Models and Symmetric Galerkin Boundary Element Method*, Ph.D. thesis, Politecnico Milano, Milan, Italy, 1999.
[55] A. Salvadori, *Analytical integrations of hypersingular kernel in* $3D$ *BEM problems*, Comput. Methods Appl. Mech. Engrg., 190 (2001), pp. 3957–3975.
[56] A. Salvadori, *Analytical integrations in* $2D$ *BEM elasticity*, Internat. J. Numer. Methods Engrg., 53 (2002), pp. 1695–1719.
[57] A. H. Schatz, V. Thomée, and W. L. Wendland, *Mathematical Theory of Finite and Boundary Element Methods*, Birkhäuser, Basel, Boston, Berlin, 1990.

[58] S. Sirtori, *General stress analysis method by means of integral equations and boundary elements*, Meccanica, 14 (1979), pp. 210–218.

[59] S. Sirtori, G. Maier, G. Novati, and S. Miccoli, *A Galerkin symmetric boundary element method in elasticity: Formulation and implementation*, Internat. J. Numer. Methods Engrg., 35 (1992), pp. 255–282.

[60] V. Sladek and J. Sladek, eds., *Singular Integrals in Boundary Element Methods*, Advances in Boundary Elements, Computational Mechanics Publications, Southampton, UK, 1998.

[61] A. Sutradhar, G. H. Paulino, and L. J. Gray, *Symmetric Galerkin boundary element method for heat conduction in functionally graded materials*, Internat. J. Numer. Methods Engrg., to appear.